MSDE

Check for updates

Preferential orientation of anisotropic polythiophene rods toward macroscopic chain ordering†

Takashi Kitao, [iD] [ab] Alexandre Legrand, [iD] [c] Taizo Mori, [de] Katsuhiko Ariga [iD] [df] and Takashi Uemura [iD] *[a]

The orientation of polymer chains plays an important role in governing the mechanical, optical, and electronic properties of polymeric materials. Here, we report on the fabrication of anisotropic polythiophene particles with controlled lengths using a metal–organic framework template, in which the alignment of the polymer chains was retained without a host support. The formation of the rod-shaped particles with long length allowed for the facile preferential orientation of the polymer particles, and consequently resulted in the macroscopic chain alignment of unprocessable polythiophene.

Design, System, Application

Several methods have so far been developed to align polymer chains, such as mechanical stress on cast films and electron spinning. However, these strategies often require the dissolution or melting of the polymers, excluding insoluble and non-melting polymers from the conventional polymer chain alignment. Here, we disclose a versatile method for the chain alignment of an unprocessable polymer using a combination of metal–organic framework (MOF) template and rubbing methods. $[In(OH)(2\text{-bromo-1,4-benzenedicarboxylate})]_n$ was employed as the host because the long-axis length of the MOF crystals could be controlled using the coordination modulation method. The anisotropic unsubstituted polythiophene rods were successfully obtained using the MOF as a template. We found that the long polymer rods could be easily aligned by mechanical rubbing treatment, achieving chain ordering at the macroscopic scale. In principle, this methodology can be extended to a wide range of unprocessable polymers. The ability of our designed system will facilitate the generation of a family of polymeric nanomaterials with highly anisotropic functions, beneficial for optical and electronic applications.

Introduction

Particle shape plays a pivotal role in determining the application of polymeric materials. Anisotropic rod-shaped polymer particles have attracted attention owing to their promising properties for optical, electronic, and biological applications.[1–9] However, engineering of anisotropy at the macroscale remains challenging, because once the particles aggregate, the resulting agglomerates cannot exhibit inherent anisotropic properties. Consequently, methods involving both controlled synthesis and unidirectional alignment of the polymer rods are in high demand to exploit the full potential advantages of their functions.

One simple yet powerful methodology for controlling the morphology of polymer particles and enabling the production of novel geometrical polymer particles involves transferring the shape pattern from host materials.[10–14] Metal–organic frameworks are highly crystalline materials with permanent porosity and tunable pore size at the molecular levels, making them attractive for a large scope of applications such as gas storage, sensing, drug delivery, separation, and catalysis.[15–23] MOF nanochannels can be used for the polymerization of accommodated monomers and provide regulated primary and higher-order structures of polymeric nanomaterials.[24–27] The MOF particle size can be tuned by the addition of capping additives that alter the coordination equilibrium at the crystal surface.[28–31] Furthermore, the host materials can be easily removed under mild conditions owing to the noncovalent framework structures. Hence, MOFs are excellent porous templates for the production of well-defined polymer particles.[32–37]

Polythiophenes have been gaining attention owing to their potential applications in nonlinear optics and electronic

[a] *Department of Applied Chemistry, Graduate School of Engineering, The University of Tokyo, Tokyo 113-8656, Japan. E-mail: uemurat@g.ecc.u-tokyo.ac.jp*

[b] *PRESTO, Japan Science and Technology Agency (JST), 4-1-8 Honcho, Kawaguchi, Saitama 332-0012, Japan*

[c] *Institute for Integrated Cell-Material Sciences (iCeMS), Kyoto University, Yoshida, Sakyo-ku, Kyoto 606-8501, Japan*

[d] *International Center for Materials Nanoarchitectonics, National Institute for Materials Science, 1-1 Namiki, Tsukuba, Ibaraki 305-0044, Japan*

[e] *Institute for Solid State Physics, The University of Tokyo, 5-1-5 Kashiwanoha, Kashiwa, Chiba 277-8581, Japan*

[f] *Graduate School of Frontier Sciences, The University of Tokyo, 5-1-5 Kashiwanoha, Kashiwa, Chiba 277-0827, Japan*

† Electronic supplementary information (ESI) available. See DOI: https://doi.org/10.1039/d2me00204c

316 | *Mol. Syst. Des. Eng.*, 2023, **8**, 316–322

This journal is © The Royal Society of Chemistry and IChemE 2023

devices.[38] Their conductivity and anisotropic optical functions can be enhanced through the alignment of the polymer chains, which can improve the device performance.[39] Our group has previously reported the fabrication of unsubstituted polythiophene (PTh) rods using a MOF host with one-dimensional nanochannels, in which the orientation of the PTh chains within the pores was not disturbed after host removal.[35] However, the size of the original host crystals could not be controlled, making it difficult to align the resulting PTh particles. Furthermore, the key to maintaining the chain orientation remains elusive. In this study, $[In(OH)(BDC-Br)]_n$ (**1**; BDC-Br = 2-bromo-1,4-benzenedicarboxylate, hexagonal channel size = 16 Å) was prepared, because the length of the host crystals can be tuned by the optimization of the synthetic conditions (*e.g.*, heating time and capping additive).[40–42] The anisotropic rod-shaped PTh particles with a controlled length was obtained using **1** as a template, in which the polymer chains were aligned along the long axis of the rods (Fig. 1). Thanks to the long length, the PTh rods could be easily aligned along a preferential direction by the mechanical rubbing treatment,[43–46] achieving the macroscopic unidirectional chain orientation (Fig. 1).

Experimental

Materials

All chemical reagents were of analytical grade, obtained from commercial suppliers (FUJIFILM Wako Pure Chemical Co., Sigma-Aldrich, Wako Chemical Co., and Tokyo Chemical Industry Co.) and used as received without further purification, unless otherwise noted. 2,2′-Azobis (isobutyronitrile) (AIBN) was recrystallized from methanol, and styrene (St) was purified by vacuum distillation before use.

Synthesis of 1

The template was synthesized and upscaled according to a previously reported protocol.[40,41] 2-Bromo-1,4-benzenedicarboxylic acid (441 mg) was dissolved in dimethylformamide (DMF, 86 mL). An $In(NO_3)_3 \cdot 3H_2O$ (710 mg) was dissolved in DMF (4 mL) and then added to the organic linker solution. The longer rod particles were obtained upon heating at 100 °C for 16 h. The particles with shorter lengths
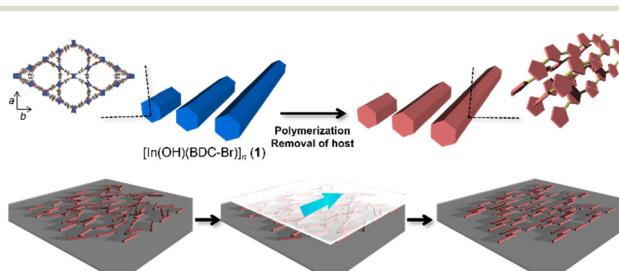
were prepared by heating the solution at 100 °C for 10 min in the presence of pyridine (158 mg) as a modulator. The obtained products were isolated by filtration and washed several times with DMF and methanol before drying.

Polymerization of terthiophene (TTh) in 1

Dried host **1** was prepared by heating at 150 °C for 12 h *in vacuo* (<0.2 kPa) in a Pyrex reaction tube. TTh (50 mg) was mixed with the degassed MOF (100 mg) in a flask. This flask was evacuated, sealed, and heated prior to heating at 180 °C for 1 h, followed by heating at 180 °C under vacuum (<0.2 kPa) for 2 h to obtain the nanocomposite of **1** with TTh. The composite was mixed with I_2 (108 mg) in a flask. The flask was then evacuated (<0.2 kPa), sealed, and subsequently heated at 90 °C for 12 h to perform the oxidative polymerization of TTh and obtain the **1**-PTh composite (**1** ⊃ PTh). After cooling to room temperature, **1** ⊃ PTh was dispersed in methanol (50 mL) and acetone (50 mL) and then dried in a Schlenk tube at 150 °C for 12 h under vacuum.

Polymerization of styrene (St) in 1

1 was heated in a Pyrex reaction tube at 150 °C for 12 h under vacuum (<0.2 kPa) to fully degas the sample. A mixture of St (1 mL) and AIBN (2 mg) added to the flask at room temperature. The mixture was left to stand for 60 min to insertion of the monomer and the initiator into **1**, after which excess external St was removed under reduced pressure (0.2 kPa) for 1.5 h at room temperature. The **1**-St nanocomposite was heated with AIBN at 95 °C for 48 h. The resulting **1** and polystyrene (PSt) composite (**1** ⊃ PSt) was obtained after washing with methanol and drying under vacuum.

Liberation of the polymers from the template

The MOF/polymer composites (100 mg) were stirred overnight in a 0.05 M aqueous solution of sodium ethylenediaminetetraacetate (Na-EDTA) for the dissolution of **1**. The collected polymers (PTh: 30 mg, PSt: 27 mg) were washed with water and methanol and dried under reduced pressure at room temperature.

Vortex flowing method

A suspension of the polymer particles in isopropanol (0.5 mg mL^{-1}, 500 μL) was added dropwise to the surface of water in a beaker (100 mL) under constant stirring at 150 rpm. After the evaporation of isopropanol, the particles were transferred using tweezers onto glass substrates.

Mechanical rubbing of the polymer particles

The PTh particle suspension in isopropanol (0.5 mg mL^{-1}, 20 μl) was dropped onto the glass substrates and dried for 30 min at room temperature. The PTh particles on the substrate was rubbed 20 times in one direction with cover glass (18 × 18 mm, Matsunami Glass Co.).

Fig. 1 Schematic image for synthesis of anisotropic PTh particles using a MOF as a template and long-range alignment of polymer rods for macroscopic chain ordering.

Visual orientation analysis

The orientation of the polymer particles was evaluated using the OrientationJ Java plugin of ImageJ (Biomedical Imaging Group, EPFL, Switzerland).[47] The structure tensor for each pixel was calculated by computing the pixel intensity gradients in the x- and y-directions within a Gaussian-shaped window.

Physical measurements

X-ray powder diffraction (XRPD) data were collected using a Rigaku SmartLab diffractometer equipped with a Cu anode. Solid-state nuclear magnetic resonance (NMR) measurements were conducted using a 9.4 T Bruker solid-state NMR instrument with an ADVANCE III 400 MHz spectrometer. ^{13}C cross-polarization magic angle spinning spectra were obtained using a double-resonance magic angle spinning probe (4 mm) with a recycle delay and spinning rate of 2 s and 6 kHz, respectively. The ^{1}H-NMR spectrum was obtained using a JEOL A-500 spectrometer operating at 500 MHz. UV-vis spectra were recorded on a JASCO V-670 spectrometer. The adsorption isotherms of N_2 were obtained at 77 K using BELSORP-mini equipment. Before the adsorption measurements, the samples were treated under reduced pressure ($<10^{-2}$ Pa) at 100 °C for 5 h. Matrix-assisted laser deposition/ionization time-of-flight mass spectrometry (MALDI-TOF MS) spectra were recorded on an Ultraflex instrument (Bruker Daltonics) using TTh as the matrix. The thermogravimetric (TG) analysis was carried out from room temperature to 500 °C at a heating rate of 10 °C min^{-1} using a Rigaku Instrument Thermo plus TG 8120 in a nitrogen atmosphere. Field-emission scanning electron microscopy (FE-SEM) images were obtained using a Hitachi SU5000 FE-SEM unit. The samples were placed on a conducting carbon tape attached to an SEM grid. Energy-dispersive X-ray spectroscopy (EDX) was performed at 28 kV and at a working distance of 10 mm. Gel permeation chromatography (GPC) measurements of the PSt were performed in CHCl$_3$ at 40 °C on three linear PSt gel columns (Shodex K-805L) connected to a JASCO PU-980 precision pump, JASCO RI-930 refractive index detector, and JASCO UV-970 UV/vis detector set at 256 nm. Transmission electron microscopy (TEM) images and selected-area electron diffraction patterns were obtained using a transmission electron microscope (JEOL, JEM-2100). The PTh dispersion in methanol was dropped and dried on a holey plastic film with a Cu mesh.

Results and discussion

Fabrication of the anisotropic polymer particles

The MOF **1** is built up by the connection of metal-centered octahedral unit InO$_4$(OH)$_2$ with BDC-Br to form the Kagome net (Fig. 1).[40] The addition of pyridine blocked the c-axis-oriented growth of the crystals, as pyridine reversibly coordinated to the In center exposed on the hexagonal facet of **1**.[48] The SEM images revealed that the long-axis length of the MOF crystals was successfully controlled using the

modulation method (Fig. 2; average long-axis length: 2.6 ± 0.18, 30.1 ± 5.98 μm).

The synthesis of PTh was conducted by the oxidative polymerization of TTh as a monomer in the nanochannels of **1**.[35] TTh was introduced into **1** by the sublimation method, affording **1** and TTh composites (**1** ⊃ TTh). **1** ⊃ TTh was then exposed to I_2 vapor for the oxidative polymerization of TTh within the nanochannels. The XRPD measurements of the nanocomposite of **1**, including PTh (**1** ⊃ PTh), indicated that the crystal structures were maintained during polymerization (Fig. 3a). The N_2 adsorption isotherm of **1** ⊃ PTh indicated a drastic decrease in the amount of adsorption compared to that of **1** (Fig. 3b). The morphology (size, shape, and surface) of **1** did not change after polymerization (Fig. 4). SEM-EDX elemental mapping measurements demonstrated the homogeneous distribution of the PTh chains in the MOF crystals (Fig. S1†). These results indicated that the polymerization of TTh proceeded inside the nanochannels of **1**.

PTh was liberated from **1** by the removal of the host in an aqueous solution of Na-EDTA. Solid-state ^{13}C-NMR and MALDI-TOF-MS analyses confirmed the formation of PTh without branching (Fig. S2 and S3†).[49] SEM-EDX analysis demonstrated the absence of the In element, thus indicating the complete removal of **1** (Fig. S1†), which was further confirmed by the absence of the diffraction peaks corresponding to residues of **1** in the XRPD pattern (Fig. 3a). The SEM images of the isolated PTh revealed that the polymer particles retained the morphology and size of the original host template, despite the removal of a large fraction of the composite mass (Fig. 4). The length of the PTh particles would have a profound effect on not only their orientation degree but also anisotropic functions (ex. conductivity, luminescence, and nonlinear optical effect).[50] The crystal growth of the MOF particles was regulated by the modulation method (Fig. 2), which allowed for the fabrication of the PTh rods with a controlled length *via* replication of the host crystals (Fig. 4e and f).
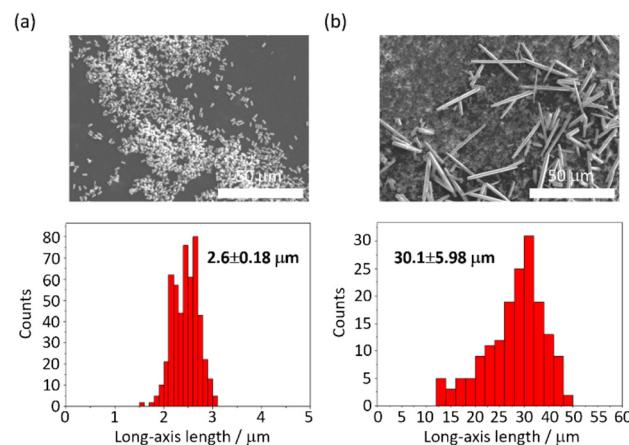
Fig. 2 SEM images and size distributions (± their standard deviations) of **1** (a) with and (b) without pyridine.

318 | *Mol. Syst. Des. Eng.*, 2023, **8**, 316–322

This journal is © The Royal Society of Chemistry and IChemE 2023
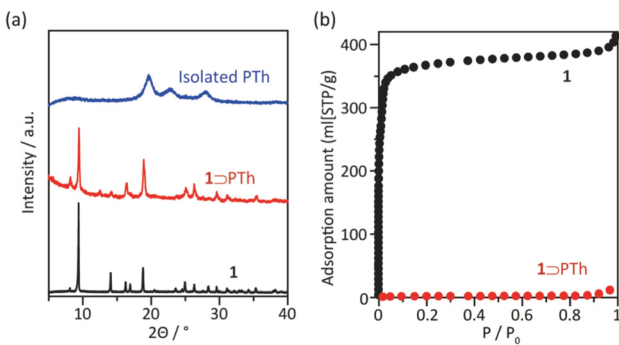
Fig. 3 (a) XRPD patterns of **1**, **1** ⊃ PTh, and PTh liberated from **1**. (b) N_2 adsorption isotherms of **1** and **1** ⊃ PTh at 77 K (**1**; S_{BET} = 1447 m^2 g^{-1}, **1** ⊃ PTh; S_{BET} = 4 m^2 g^{-1}).
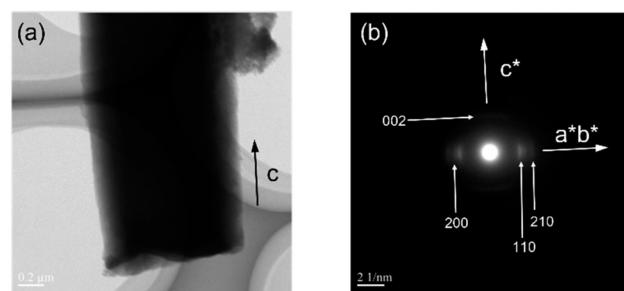
Fig. 5 (a) TEM image and (b) selected area electron diffraction patterns of PTh from **1**.

Microstructure of the polymer chains

Further characterization of the polymer particles revealed the microstructures of the polymer chains. The XRPD analysis of the isolated PTh showed characteristic peaks of crystalline PTh with a herringbone packing structure, thus indicating its reorganization into a crystalline configuration (Fig. 3a). As the direction of crystal growth in **1** was parallel to the *c*-axis, the polymer chains were predicted to be aligned along the long axis of the obtained polymer rod particles, as previously reported.[35] The selected-area electron diffraction patterns *via* the TEM images were analyzed, and the diffraction spots indexed as (*xy*0) and (002) in the directions perpendicular and parallel to the long axis of the polymer particle, respectively, were visualized (Fig. 5). The (002) diffraction peak corresponded to the lattice plane perpendicular to the axis of the polymer backbone, indicating that the orientation of the PTh chains was not disturbed after digesting the host matrices even though PTh is a linear polymer without cross-linking. The UV-vis spectra revealed that the PTh chains

formed well-ordered conjugated segments, unlike the PTh prepared by solution polymerization (Fig. S4†).[35,51]

To reveal the effects of the structural characteristics, such as backbone rigidity and flexibility, on the chain reorganization process upon host removal, particles of PSt, a nonconjugated polymer, were fabricated using **1** as a template (see the Experimental section), and their microstructures were characterized. XRPD, TG, ^{1}H-NMR, and GPC results confirmed the formation of PSt (M_n = 39 000, M_w/M_n = 2.73) (Fig. S5–S8†). The SEM images revealed that the PSt rod particles were successfully obtained upon removing the framework (Fig. S9†). Unlike in the case of PTh, a diffraction peak was not observed in the XRPD pattern of the PSt isolated from **1**; instead, diffuse scattering was observed, which is typical for amorphous atactic PSt (Fig. S5†). The electron diffraction method cannot be applied to evaluate the macromolecular orientation due to its amorphous state. The orientation of the PSt chains was examined using polarized Raman spectroscopy.[52,53] The rod samples were placed in such a manner that the long axis was parallel and perpendicular to the direction of the polarized excitation laser. The intensity of the Raman band at 623 cm^{-1} was
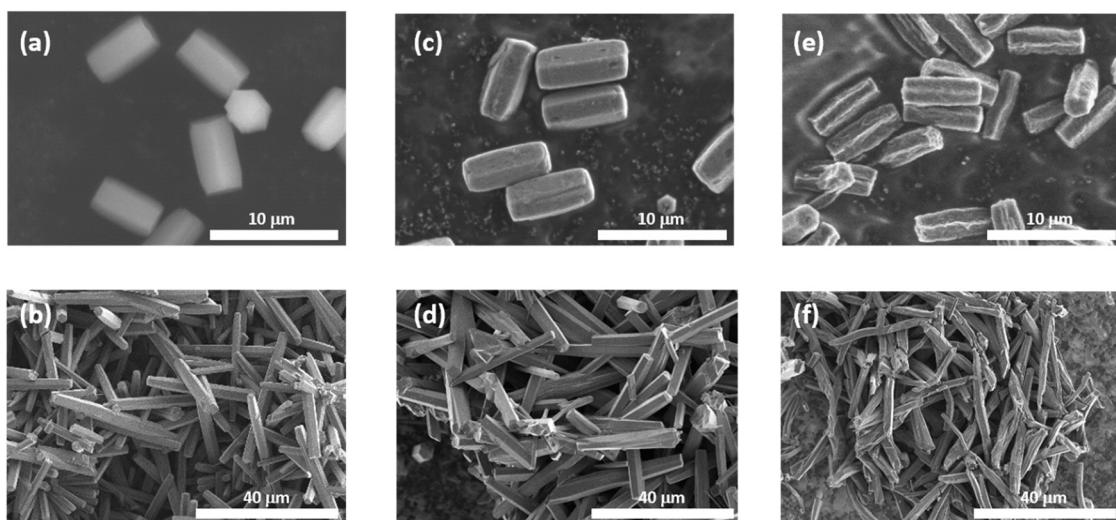

Fig. 4 SEM images of (a and b) **1** with different lengths obtained by the coordination modulation method, (c and d) **1** ⊃ PTh, and (e and f) PTh isolated from **1**. The morphologies and size of the recovered PTh objects retained those of the original hosts.

attributed to the antisymmetric skeletal vibration of the benzene ring, which is known to vary with the polarization direction.[52] The PSt particles showed similar Raman band intensities between the parallel and perpendicular directions at 623 cm^{-1}, indicating that the polymer chains were not oriented along the long-axis direction (Fig. S10†). In contrast, it should be noted that the alignment of the PTh chains was supported by the Raman spectroscopy measurements, in which the intensity of the peak at 1436 cm^{-1}, ascribable to the C=C in-phase stretching mode of thiophene, drastically changed, depending on the polarization direction of the excitation laser (Fig. S11†).[54] These results revealed that, unlike in the case of PTh, the chain orientation of PSt was not preserved after the removal of the MOF matrix. PSt had a much larger molecular weight than that of PTh (Fig. S2 and S8†), and the loading amount of PSt was almost the same as that of PTh (see the Experimental section). Consequently, it is likely that the rigidity of the polymer backbones and effective interchain interactions are essential for the orientation memory effect.

Alignment of the PTh rod particles

Although the PTh chains are oriented within each particle, their anisotropy is lost at the macroscopic scale when the particles aggregate. For uniaxial orientation of the polymer particles, a vortex Langmuir–Blodgett (vortex-LB) method was employed, whereby the vortex motion caused by the mechanical stirring of a subphase medium directs the floating particles to align at the liquid interface.[55] The dispersion of PTh particles was added dropwise to the water surface under stirring, and the resulting film was transferred onto a glass substrate. However, the PTh particles were not fully oriented, and the strong hydrophobicity of PTh resulted in the formation of random agglomerates on the surface (Fig. S12†). The PTh dispersion was then dropped onto glass substrates, and the particles were aligned using the mechanical rubbing method.[43–46] The film of the PTh rods on the substrate were rubbed using a cover glass. Strikingly, this simple method allowed for the preferential alignment of the particles. The orientation degree of the particles was analyzed before and after the rubbing treatment using the OrientationJ plugin (see the Experimental section for details). An unimodal and narrow angular distribution was obtained with longer-length PTh rods, demonstrating the orientation of the rod particles, while the shorter rod particles provided a nearly isotropic orientational distribution, presumably due to the reduced shear orientation effects (Fig. 6 and S13†).[56] These results clearly underlined the necessity to control the particle length for achieving the alignment of the particles. Several techniques have been employed to align polymer chains, such as applying mechanical stress on cast films and electrospinning;[57,58] however, these strategies mostly require the melting or dissolution of the polymers. These methods cannot be applied to PTh because strong interchain interactions render PTh nonfusible and insoluble with a
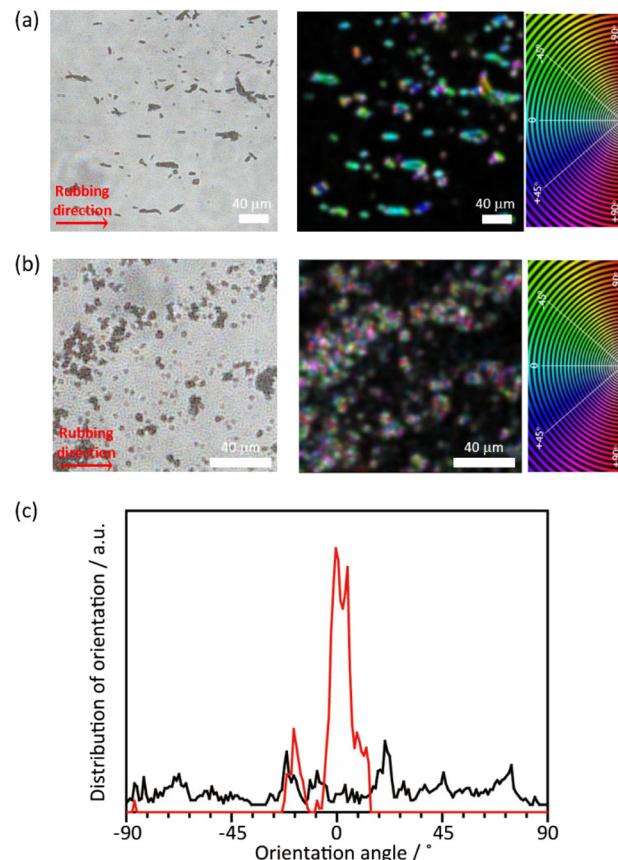
Fig. 6 (a and b) Microscope images and orientation analyses of (a) long and (b) short PTh rod particles after mechanical rubbing treatment. Orientation analyses were color-coded according to the orientation color map from −90° to +90°. (c) Angle orientation of the PTh rods with long (red) and short (black) length.

nonmelting behavior. The results of this study demonstrated that the combination of the MOF template with simple rubbing methods can result in the macroscopic alignment of unprocessable polymers.

Conclusions

In conclusion, this paper reports the fabrication of anisotropic PTh particles with tunable lengths using a MOF template. The microstructure of the polymer chains was explored by XRPD, selected-area electron diffraction, and polarized Raman spectroscopy measurements, and the results indicated that the inherent rigidity of the polymer chains as well as the inter-chain interactions were an essential prerequisite for maintaining the polymer chain alignment during recovery. Tuning the length of the rod particles allowed for the unidirectional ordering of the PTh particles by a mechanical rubbing treatment, which led to the alignment of the PTh chains at the macroscopic scale. This system can contribute to the preparation of a variety of polymeric materials with highly anisotropic functional properties for their application in advanced optoelectronic devices.[59]

Conflicts of interest

There are no conflicts to declare.

Acknowledgements

References

1 N. J. Halas, *Nano Lett.*, 2010, **10**, 3816–3822.
2 S. C. Glotzer and M. J. Solomon, *Nat. Mater.*, 2007, **6**, 557–562.
3 S. Lee, C. M. Yoon, J. Y. Hong and J. Jang, *J. Mater. Chem. C*, 2014, **2**, 6010–6016.
4 C. W. Liu, Y. C. Wei, C. C. Liu and K. W. Wang, *J. Mater. Chem.*, 2012, **22**, 4641–4644.
5 H. Wang, R. Zhao, Y. Li, H. Liu, F. Li, Y. Zhao and G. Nie, *Nanomedicine*, 2016, **12**, 439–448.
6 D. Muenmart, A. B. Foster, A. Harvey, M. T. Chen, O. Navarro, V. Promarak, M. C. McCairn, J. M. Behrendt and M. L. Turner, *Macromolecules*, 2014, **47**, 6531–6539.
7 T. Adachi, L. Tong, J. Kuwabara, T. Kanbara, A. Saeki, S. Seki and Y. Yamamoto, *J. Am. Chem. Soc.*, 2013, **135**, 870–876.
8 A. J. C. Kuehne, M. C. Gather and J. Sprakel, *Nat. Commun.*, 2012, **3**, 1088.
9 S. I. Moon and T. J. McCarthy, *Macromolecules*, 2003, **36**, 4253–4255.
10 P. Sozzani, S. Bracco, A. Comotti, R. Simonutti, P. Valsesia, Y. Sakamoto and O. Terasaki, *Nat. Mater.*, 2006, **5**, 545–551.
11 G. Distefano, A. Comotti, S. Bracco, M. Beretta and P. Sozzani, *Angew. Chem., Int. Ed.*, 2012, **51**, 9258–9262.
12 J. F. Hulvat and S. I. Stupp, *Angew. Chem., Int. Ed.*, 2003, **42**, 778–781.
13 D. Park, B. Kim, M. Jang, K. Bae and J. Joo, *Appl. Phys. Lett.*, 2005, **86**, 113116.
14 J. I. Lee, S. H. Cho, S.-M. Park, J. K. Kim, J. K. Kim, J.-W. Yu, Y. C. Kim and T. P. Russell, *Nano Lett.*, 2008, **8**, 2315–2320.
15 K. Sumida, D. L. Rogow, J. A. Mason, T. M. McDonald, E. D. Bloch, Z. R. Herm, T.-H. Bae and J. R. Long, *Chem. Rev.*, 2011, **112**, 724–781.
16 S. Kitagawa, R. Kitaura and S. I. Noro, *Angew. Chem., Int. Ed.*, 2004, **43**, 2334–2375.
17 R. J. Kuppler, D. J. Timmons, Q.-R. Fang, J.-R. Li, T. A. Makal, M. D. Young, D. Yuan, D. Zhao, W. Zhuang and H.-C. Zhou, *Coord. Chem. Rev.*, 2009, **253**, 3042–3066.
18 G. Férey, *Chem. Soc. Rev.*, 2008, **37**, 191–214.
19 H. Furukawa, K. E. Cordova, M. O'Keeffe and O. M. Yaghi, *Science*, 2013, **341**, 1230444.
20 X. Zhao, X. Song, Y. Li, Z. Chang and L. Chen, *ACS Appl. Mater. Interfaces*, 2018, **10**, 5633–5640.
21 H. Miyasaka, *Bull. Chem. Soc. Jpn.*, 2021, **94**, 2929–2955.
22 N. Hosono, *Bull. Chem. Soc. Jpn.*, 2021, **94**, 60–69.
23 M. Takahashi, *Bull. Chem. Soc. Jpn.*, 2021, **94**, 2602–2612.
24 N. Ding, H. Li, X. Feng, Q. Wang, S. Wang, L. Ma, J. Zhou and B. Wang, *J. Am. Chem. Soc.*, 2016, **138**, 10100–10103.
25 T. Kitao, Y. Zhang, S. Kitagawa, B. Wang and T. Uemura, *Chem. Soc. Rev.*, 2017, **46**, 3108–3133.
26 H.-C. Lee, M. Antonietti and B. V. Schmidt, *Polym. Chem.*, 2016, **7**, 7199–7203.
27 N. Hosono and T. Uemura, *Bull. Chem. Soc. Jpn.*, 2021, **94**, 2139–2148.
28 S. Furukawa, J. Reboul, S. Diring, K. Sumida and S. Kitagawa, *Chem. Soc. Rev.*, 2014, **43**, 5700–5734.
29 T. Tsuruoka, S. Furukawa, Y. Takashima, K. Yoshida, S. Isoda and S. Kitagawa, *Angew. Chem., Int. Ed.*, 2009, **48**, 4739–4743.
30 A. Umemura, S. Diring, S. Furukawa, H. Uehara, T. Tsuruoka and S. Kitagawa, *J. Am. Chem. Soc.*, 2011, **133**, 15506–15513.
31 S. Diring, S. Furukawa, Y. Takashima, T. Tsuruoka and S. Kitagawa, *Chem. Mater.*, 2010, **22**, 4531–4538.
32 T. Ishiwata, Y. Furukawa, K. Sugikawa, K. Kokado and K. Sada, *J. Am. Chem. Soc.*, 2013, **135**, 5427–5432.
33 M. Tsotsalas, J. Liu, B. Tettmann, S. Grosjean, A. Shahnas, Z. Wang, C. Azucena, M. Addicoat, T. Heine, J. Lahann, J. Overhage, S. Bräse, H. Gliemann and C. Wöll, *J. Am. Chem. Soc.*, 2014, **136**, 8–11.
34 T. Uemura, T. Kaseda and S. Kitagawa, *Chem. Mater.*, 2013, **25**, 3772–3776.
35 T. Kitao, M. W. A. MacLean, B. Le Ouay, Y. Sasaki, M. Tsujimoto, S. Kitagawa and T. Uemura, *Polym. Chem.*, 2017, **8**, 5077–5081.
36 Z. G. Gu, W. Q. Fu, M. Liu and J. Zhang, *Chem. Commun.*, 2017, **53**, 1470–1473.
37 M. W. MacLean, T. Kitao, T. Suga, M. Mizuno, S. Seki, T. Uemura and S. Kitagawa, *Angew. Chem., Int. Ed.*, 2016, **55**, 708–713.
38 J. Roncali, *Chem. Rev.*, 1992, **92**, 711–738.
39 D. Kajiya, S. Ozawa, T. Koganezawa and K.-I. Saitow, *J. Phys. Chem. C*, 2015, **119**, 7987–7995.
40 C. Volkringer, M. Meddouri, T. Loiseau, N. Guillou, J. Marrot, G. Férey, M. Haouas, F. Taulelle, N. Audebrand and M. Latroche, *Inorg. Chem.*, 2008, **47**, 11892–11901.
41 S. Choi, T. Kim, H. Ji, H. J. Lee and M. Oh, *J. Am. Chem. Soc.*, 2016, **138**, 14434–14440.
42 B. Hosseini Monjezi, B. Sapotta, S. Moulai, J. Zhang, R. Oestreich, B. P. Ladewig, K. Müller-Buschbaum, C. Janiak, T. Hashem and A. Knebel, *Chem. Ing. Tech.*, 2022, **94**, 135–144.
43 Y. Amit, A. Faust, I. Lieberman, L. Yedidya and U. Banin, *Phys. Status Solidi A*, 2012, **209**, 235–242.
44 C. Park, K. Koh and U. Jeong, *Sci. Rep.*, 2015, **5**, 8340.
45 L. Hartmann, D. Djurado, I. Florea, J.-F. Legrand, A. Fiore, P. Reiss, S. Doyle, A. Vorobiev, S. Pouget, F. Chandezon, O. Ersen and M. Brinkmann, *Macromolecules*, 2013, **46**, 6177–6186.
46 H. Eimura, A. Niwa, J. Uchida and T. Kato, *Bull. Chem. Soc. Jpn.*, 2021, **94**, 1588–1593.

47 Z. Püspöki, M. Storath, D. Sage and M. Unser, *Adv. Anat., Embryol. Cell Biol.*, 2016, **219**, 69–93.

48 L. Sun, R. Li, W. Zhan, Y. Yuan, X. Wang, X. Han and Y. Zhao, *Nat. Commun.*, 2019, **10**, 2270.

49 J. Chen, J. Shu, S. Schobloch, A. Kroeger, R. Graf, R. Muñoz-Espí, K. Landfester and U. Ziener, *Macromolecules*, 2012, **45**, 5108–5113.

50 J. Mattu, T. Johansson and G. W. Leach, *J. Phys. Chem. C*, 2007, **111**, 6868–6874.

51 P. J. Brown, D. S. Thomas, A. Köhler, J. S. Wilson, J. S. Kim, C. M. Ramsdale, H. Sirringhaus and R. H. Friend, *Phys. Rev. B: Condens. Matter Mater. Phys.*, 2003, **67**, 642031–6420316.

52 D. Papkov, C. Pellerin and Y. A. Dzenis, *Macromolecules*, 2018, **51**, 8746–8751.

53 B. Jasse and J. L. Koenig, *J. Polym. Sci., Polym. Phys. Ed.*, 1980, **18**, 731–738.

54 N. Kumari, M. Pandey, S. Nagamatsu, M. Nakamura and S. S. Pandey, *ACS Appl. Mater. Interfaces*, 2020, **12**, 11876–11883.

55 V. Krishnan, Y. Kasuya, Q. Ji, M. Sathish, L. K. Shrestha, S. Ishihara, K. Minami, H. Morita, T. Yamazaki, N. Hanagata, K. Miyazawa, S. Acharya, W. Nakanishi, J. P. Hill and K. Ariga, *ACS Appl. Mater. Interfaces*, 2015, **7**, 15667–15673.

56 M. Schlenk, E. Hofmann, S. Seibt, S. Rosenfeldt, L. Schrack, M. Drechsler, A. Rothkirch, W. Ohm, J. Breu, S. Gekle and S. Förster, *Langmuir*, 2018, **34**, 4843–4851.

57 B. O'Connor, R. J. Kline, B. R. Conrad, L. J. Richter, D. Gundlach, M. F. Toney and D. M. DeLongchamp, *Adv. Funct. Mater.*, 2011, **21**, 3697–3705.

58 M. Richard-Lacroix and C. Pellerin, *Macromolecules*, 2013, **46**, 9473–9493.

59 T. Kato, M. Gupta, D. Yamaguchi, K. P. Gan and M. Nakayama, *Bull. Chem. Soc. Jpn.*, 2021, **94**, 357–376.